RSC Advances

PAPER

View Article Online
View Journal | View Issue

Cite this: *RSC Adv.*, 2021, **11**, 33653

Vinylene-bridged donor–acceptor type porous organic polymers for enhanced photocatalysis of amine oxidative coupling reactions under visible light†

Bang Wu,[a] Xinyue Jiang,[a] Yang Liu,[a] Qiu-Yan Li,*[a] Xinsheng Zhao[b] and Xiao-Jun Wang*[a]

Porous organic polymers (POPs), owing to their abundant porosity, high stability and well-tunable properties, are promising candidates as heterogeneous photocatalysts for organic transformations. Here we report two vinylene-bridged donor–acceptor (D–A) structural POPs (TpTc-POP and TbTc-POP) that are facilely constructed by the electron-rich triarylamine and electron-deficient tricyanomesitylene as key building blocks by the organic base catalyzed Knoevenagel condensation. Both TpTc-POP and TbTc-POP possess hierarchical meso- and micro-pores with a high surface area. Furthermore, the unsubstituted vinylene linkages of D–A moieties in their polymer backbones extend their π-conjugation and render their broad absorption range in the visible-light region. Thus, these DA-POPs exhibited highly effective photocatalytic activities for aerobic oxidative coupling of amines to imines under visible light irradiation. This study shows the great potential of conjugated POPs with a D–A structural feature in designing highly efficient and active heterogeneous photocatalytic systems.

Received 13th August 2021
Accepted 9th October 2021

DOI: 10.1039/d1ra06118f

rsc.li/rsc-advances

Introduction

Visible light photoredox catalysis has gained remarkably extensive research attention in the recent decades, because it provides a sustainable and environmentally friendly method for a wide range of organic transformations.[1] Since a large proportion of organic substrates cannot absorb photons in the visible region, a variety of photocatalysts that absorb strongly in the visible spectrum are often employed in these photochemical processes, including noble metal Ru^{2+} or Ir^{3+} complexes,[2] as well as organic dyes.[3] However, these homogeneous catalytic systems would suffer from several inherent drawbacks to some extent, such as the high price and scarcity of precious metals, the photobleaching of organic dyes, and the low recyclability and reusability of photocatalysts, which impede their practical applications in scale-up synthesis. The hybridization of these photocatalysts with solid-state materials, such as metal–organic frameworks and dye doped metal oxides, only partially alleviates the difficulty of recyclability.[4] Consequently, the development of efficient heterogeneous photocatalysts that are low cost and recyclable, have outstanding catalytic activity and are free of precious metals is highly desirable.

Porous organic polymers (POPs) as a novel class of porous materials are constructed by robust covalent bonds between various organic building blocks, featuring high porosity, structural tunability and diversity, together with highly physicochemical stability.[5] They have been widely investigated in a plethora of applications, such as gas sorption/separation, chemical sensing, heterogeneous catalysis and water treatment.[5,6] Among them, conjugated POPs with extended π-conjugated skeletons have emerged as a versatile platform for efficient photocatalytic organic transformations.[7] In particular, the simultaneous introduction of electron donor and acceptor (D–A) building units into their conjugated polymer backbones can greatly enhance the visible-light harvesting capability and charge separation efficiency of photogenerated carriers, thereby resulting in an improvement of photocatalytic performance.[7,8] Moreover, these properties also are closely related to the intrinsic chemical linkage of D–A building units in conjugated POPs.

Among the various linkages in POPs, sp^2 carbon vinylene C=C linkage that can enhance both of the chemical stability and π-electron delocalization of conjugated polymer skeletons has witnessed a rapidly increasing attention since the first report in 2016.[9,10] These unique features make vinylene-linked POPs emerging as promising heterogeneous photocatalysts in a diverse array of photocatalytic applications along with improved photocatalytic performance in comparison to their

[a]Jiangsu Key Laboratory of Green Synthetic Chemistry for Functional Materials, School of Chemistry and Materials Science, Jiangsu Normal University, Xuzhou 221116, P. R. China. E-mail: xjwang@jsnu.edu.cn; qyli@jsnu.edu.cn

[b]School of Physics and Electronic Engineering, Jiangsu Normal University, Xuzhou 221116, P. R. China

† Electronic supplementary information (ESI) available. See DOI: 10.1039/d1ra06118f

analogues with other dynamic linkages.[11] For example, Zhang and co-workers employed electron-deficient tricyanomesitylene moiety as a key building block to obtain various olefin-bridged conjugated porous polymers or covalent organic frameworks, which exhibited highly photocatalytic activities for water-splitting reactions or aerobic oxidation of arylboronic acids.[12] Wang's group utilized electron-accepting benzothiadiazole and electron-donating pyrene to construct a donor–acceptor sp^2-carbon-linked covalent organic framework for efficient photocatalytic thioamide cyclization and oxidative amine coupling.[13]

However, in this regard, there are still only limited reports regarding vinylene-bridged donor–acceptor structural POPs to date. Thus, it is in high demand to couple various polyarene building blocks into these POPs in order to finely tune their photophysical and electronic properties. Here, we report two vinylene-linked D–A structural POPs composed of triarylamine donor and tricyanomesitylene acceptor (termed as TpTc-POP and TbTc-POP). Due to the extended π-conjugation of D–A units in polymer backbones, they exhibited highly photocatalytic activities for visible-light-driven aerobic oxidative coupling of amines to imines.

Results and discussion

Triphenylamine (TPA) and its derivatives are well-known photoactive molecules along with excellent electron-donating abilities, and they have been widely used in various optoelectronic materials.[14] Thus, electron-rich TPA motif based aldehydes [*i.e.* tris(4-formylphenyl)amine (TFPA) or tris[1-(1′-formyl-4,4′-biphenyl)]amine (TFBA)] was used to readily react with electron-deficient tricyanomesitylene (TCM) by organic base piperidine catalyzed Knoevenagel condensation at 150 °C for 72 h in DMF, resulting in the formation of two vinylene-bridged D–A structural POPs TpTc-POP and TbTc-POP as depicted in Scheme 1. Besides, in order for comparison, the model compound (termed as DpTc) and control POP (termed as TfTc-POP) were prepared by reacting TCM with *p*-(diphenylamino) benzaldehyde and 1,3,5-tris(*p*-formylphenyl)benzene under the similar reaction conditions, respectively (Schemes S1 and S2 in ESI†).

The chemical structures of TpTc-POP and TbTc-POP were confirmed by solid-state ^{13}C cross-polarization/magic angle spinning (CP/MAS) nuclear magnetic resonance (NMR) and Fourier transform infrared (FT-IR) spectral analyses. As shown in Fig. 1a, the ^{13}C CP/MAS NMR of TpTc-POP and TbTc-POP are combined and compared with ^{13}C NMR spectra of model compound DpTc in $CDCl_3$. The peaks at around 115 ppm were assigned to cyano groups (c). The most intense signals at 128 ppm were ascribed to the newly formed olefinic carbon (a) overlapped with aromatic carbons (h). The broad peaks at around 148 ppm were attributed to a combination of the carbon

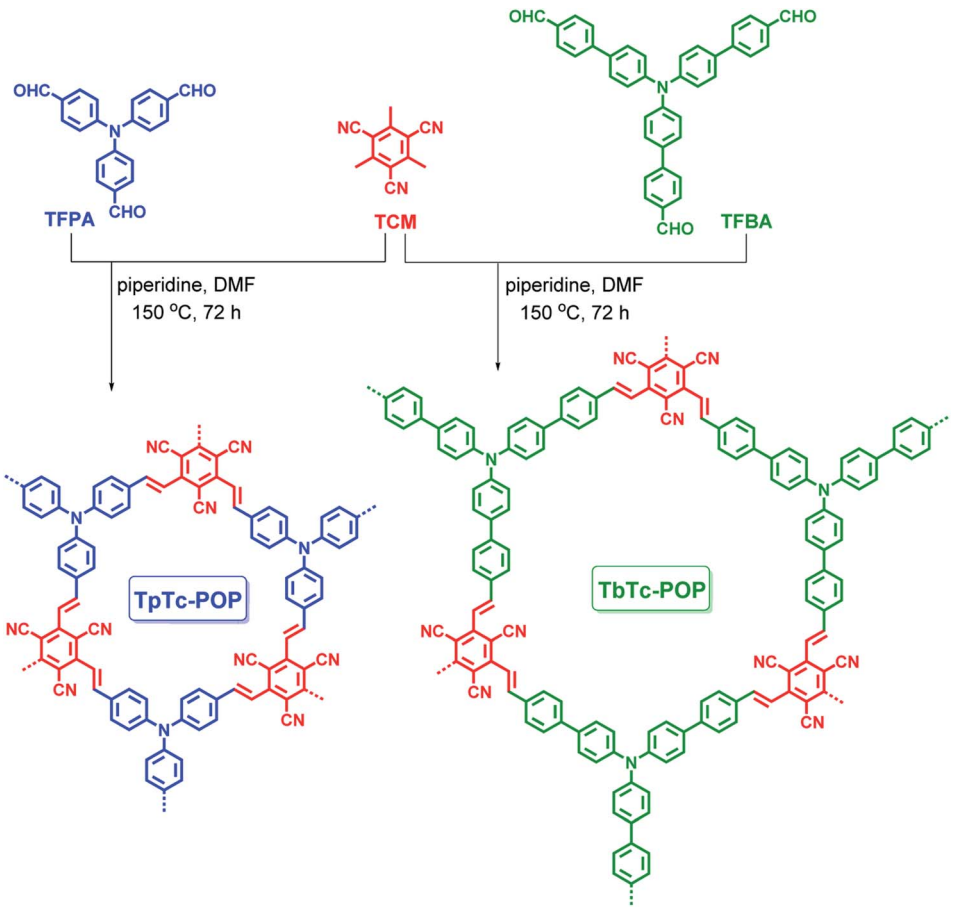

Scheme 1 Synthetic routes of vinylene-bridged D–A porous organic polymers TpTc-POP and TbTc-POP.

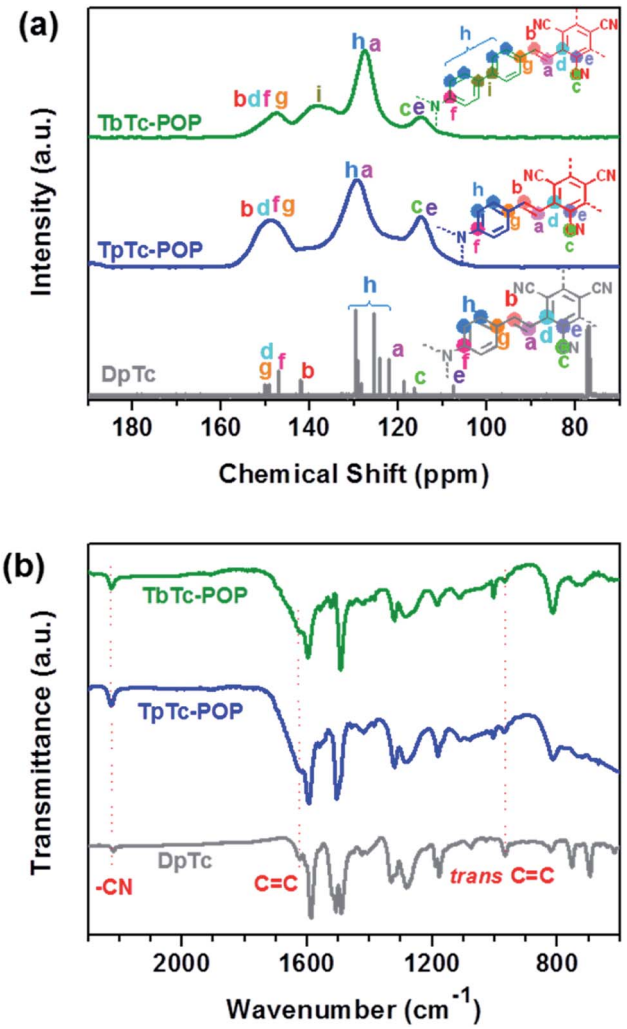

Fig. 1 Solid-state ^{13}C CP/MAS NMR (a) and FT-IR (b) spectra of TpTc-POP, TbTc-POP and the model compound DpTc.

atoms (b, d, f and g) in POPs. Furthermore, FT-IR spectra of TpTc-POP and TbTc-POP revealed the stretching vibration signals of newly formed C=C moieties at 1626 and 970 cm^{-1} in both POPs, verifying the presence of the *trans*-formed vinylene linkages in the as-prepared POP skeletons (Fig. 1b). The peak at 2226 cm^{-1} was attributed to the stretching vibration of cyano group (CN). Moreover, the peaks at *ca.* 1700 cm^{-1} corresponding to C=O stretching vibration of aldehyde monomers disappeared in POP samples, indicative of their high polymerization degrees (Fig. S1 in ESI†). The morphologies of POPs examined by scanning electron microscopy (SEM) revealed their nanoscale particles in a relatively tight texture (Fig. S2 in ESI†). Powder X-ray diffraction (PXRD) profiles of TpTc-POP and TbTc-POP indicated their amorphous nature with the broad peaks at around 20°, suggesting the partial π–π stacked structure in polymer skeletons (Fig. S3 in ESI†). On the other hand, we have tried to optimize the reaction conditions in order to obtain the crystalline frameworks for these two POPs. However, no desirable results were achieved at present stage. This should be ascribed to the conformation of TPA unit, in which three phenyl rings are not in the same plane. Thermogravimetric analysis (TGA) revealed that they possessed favorable stability up to 400 °C with only 5–10% weight loss under a nitrogen atmosphere (Fig. S4 in ESI†). These results strongly supported the facile formation of target vinylene-linked D–A conjugated polymers by efficient polycondensation of TPA aldehydes and tricyanomesitylene.

As shown in Fig. 2, the porosities and specific surface areas of TpTc-POP and TbTc-POP were characterized by nitrogen sorption isotherms measured at 77 K. Both of them displayed a combination of type I and IV nitrogen sorption isotherms according to the IUPAC classification,[15] suggesting the co-existence of micropores and mesopores in two POPs. The obtained curves showed a steep increase at low pressure of $P/P_0 <$ 0.1, corresponding to their microporous nature. And the desorption hysteresis at high pressure was attributed to the extensive mesopores. Besides, the Brunauer–Emmett–Teller (BET) surface area was calculated to be 966 and 538 m^2 g^{-1} for TpTc-POP and TbTc-POP, respectively. The nonlocal density functional theory (NLDFT) was utilized to calculate their pore-size distributions, which revealed two type of micro- and meso-porous distribution of 0.78, 1.69, 5.25 nm for TpTc-POP and 0.84, 1.73, 5.26 nm for TbTc-POP, respectively. Their hierarchical porous structures are beneficial for the diffusion and transformation of substrates in the photocatalytic process.

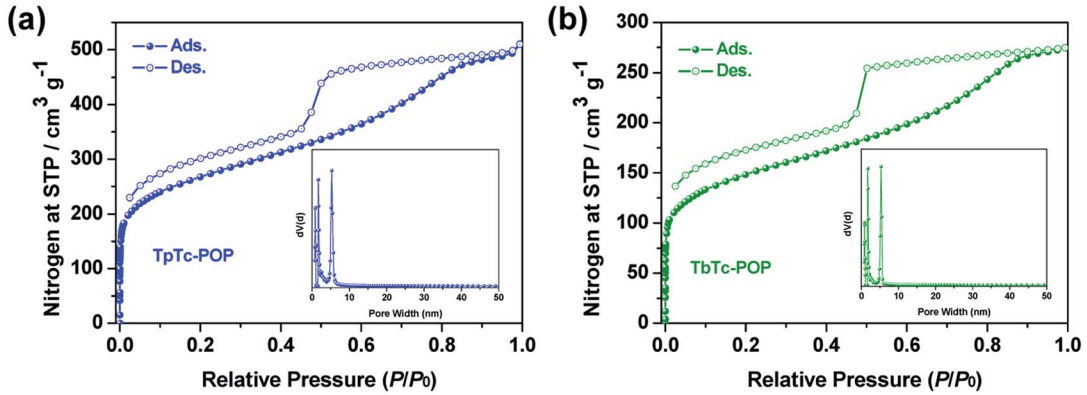

Fig. 2 Nitrogen adsorption and desorption isotherms of TpTc-POP (a) and TbTc-POP (b). Insets: the pore size distributions derived from NLDFT.

The electronic structures of TpTc-POP, TbTc-POP and the control TfTc-POP were studied by ultraviolet-visible diffuse reflectance spectroscopy (UV-vis DRS) and ultraviolet photoelectron spectroscopy (UPS). As shown in Fig. 3a, their UV-vis DRS showed a similar absorption range with a maximum of 300–600 nm and a gradual decrease until even near infrared around 900 nm. Accordingly, their optical band gaps were calculated from Kubelka–Munk function as 1.93, 1.95, and 1.98 eV for TpTc-POP, TbTc-POP and TfTc-POP, respectively (Fig. 3b). These results confirmed their strong visible-light harvesting abilities and low band gap characters caused by the extended sp^2-carbon π-conjugation of D–A units in polymer backbones.[7,8] Besides, the solid samples of POPs exhibited a photoluminescence (PL) band with a maximum peak centered at 585 nm for TfTc-POP, 638 nm for TbTc-POP and 650 nm for TpTc-POP, respectively (Fig. 3c). Their PL decay curves are fitted with the average lifetimes of 1.7 ns for TfTc-POP, 2.9 ns for TbTc-POP and 3.2 ns for TpTc-POP (Fig. S5 in ESI†). In comparison to TfTc-POP, the distinct PL redshifted by over 50 nm and the elongated lifetimes of TpTc-POP and TbTc-POP should be attributed to the stronger electron-donating ability of TPA units in polymers, thus, benefitting the charge separation of D–A components.

Furthermore, the energy of valence band maximum (E_{VB} in relative to the vacuum level) of TpTc-POP, TbTc-POP and TfTc-POP were evaluated by UPS analyses to be −5.6, −5.5, and −6.0 eV, respectively (Fig. 3d and S6 in ESI†). Thereby, the energy of the conduction band minimum (E_{CB}) of TpTc-POP,

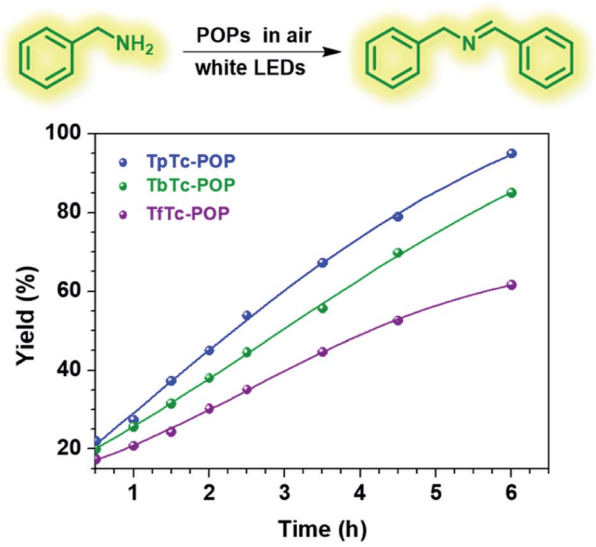

Fig. 4 Oxidative coupling of benzylamine to imine over time with different POP photocatalysts under the irradiation of white-LEDs in an open air atmosphere.

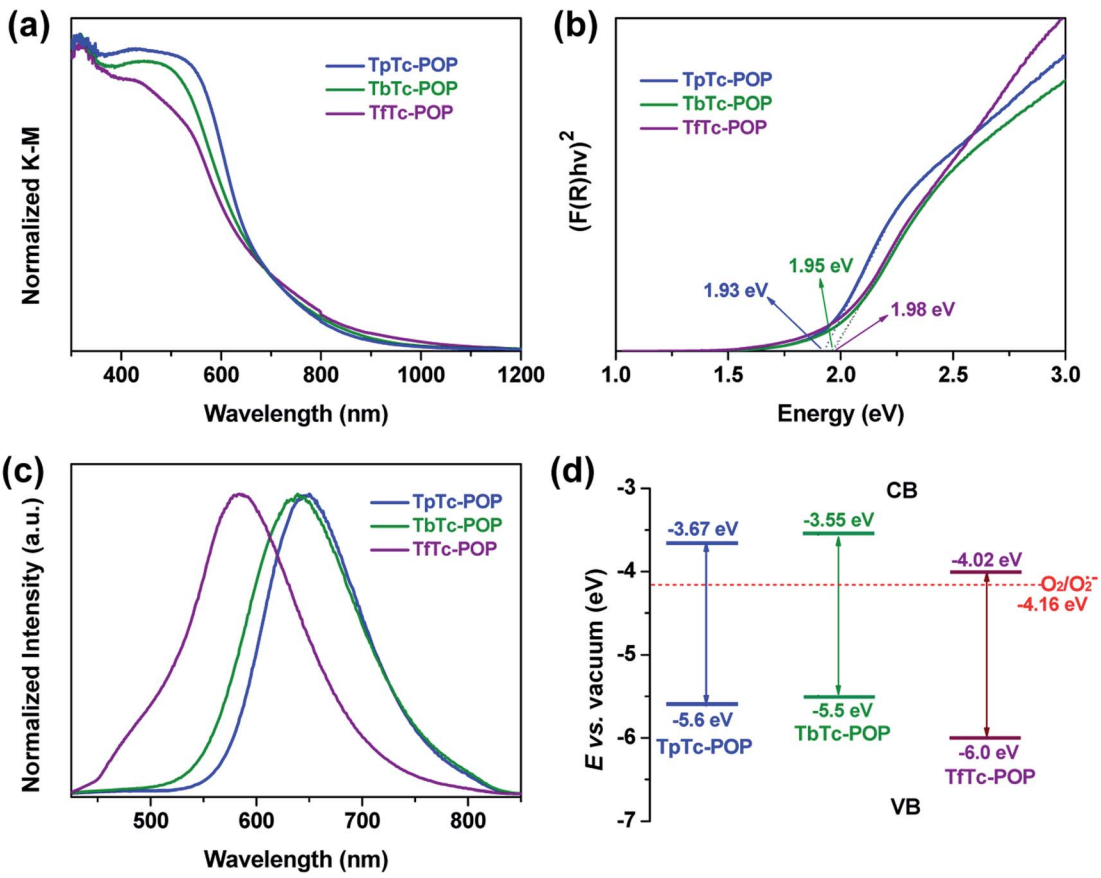

Fig. 3 (a) UV-vis diffuse reflectance spectra of TpTc-POP, TbTc-POP and control TfTc-POP. (b) The corresponding band gaps determined from the Kubelka–Munk-transformed reflectance spectra. (c) Photoluminescence spectra of TpTc-POP, TbTc-POP and control TfTc-POP measured in the solid state. (d) Band structures and the thermodynamic equilibrium redox potential for O_2 in vacuum scale.

Table 1 Photocatalytic aerobic oxidative coupling reaction of benzylamine by TpTc-POP[a]

	Entry						
	1	2	3	4[c]	5[d]	6[e]	7[f]
TpTc-POP	+	+	—	+	+	+	+
hv	+	—	+	+	+	+	+
Air	+	+	+	—	+	+	+
Yield[b] (%)	95	Trace	Trace	Trace	11	47	20

[a] Reaction conditions: benzylamine (0.5 mmol), TpTc-POP (5 mg), solvent acetonitrile (1.5 mL), 6 h, white LEDs (3 W, ~100 mW cm^{-2}), room temperature. [b] Determined by ^{1}H-NMR analysis. [c] Under nitrogen atmosphere. [d] KI as the hole scavenger. [e] NaN_3 as the single oxygen $^1O_2$ scavenger. [f] *p*-Benzoquinone as the superoxide scavenger.

TbTc-POP and TfTc-POP were calculated as −3.67, −3.55 and −4.02 eV, respectively. Since the E_{CB} of all three POPs are higher than the potential of $O_2/O_2^{\bullet-}$ (−4.16 eV), they allowed for the reduction of oxygen to a superoxide radical anion upon photoexcitation.[1,16]

Encouraged by these POPs' photoelectronic properties, we thus evaluated and compared their photocatalytic activities by using visible light-driven aerobic oxidative coupling of benzylamine to imine as a model reaction. As shown in Fig. 4, the photocatalytic reactions with 1 mol% POPs loading in acetonitrile were performed in an open air atmosphere under white LEDs irradiation at room temperature and the progresses were monitored by ^{1}H NMR. As expected, all three POPs can smoothly photocatalyze this transformation of benzylamine to imine and afford good conversions. The yields of *N*-benzylidenebenzylamine after 6 h irradiation are 95%, 85% and 62% for TpTc-POP, TbTc-POP and TfTc-POP, respectively. It is clear that TpTc-POP and TbTc-POP containing TPA moieties exhibited higher photocatalytic efficiency than their control POP TfTc-POP. This should be attributed to the fact that TPA units possess the strong electron-donating abilities. Besides, the recyclability and reusability of TpTc-POP and TbTc-POP were also examined for this photocatalytic model reaction. After they were separated by simple centrifugation from the reaction mixture, both of them remained highly active for at least five cycles (Fig. S7 in ESI†). On the other hand, nitrogen sorption isotherms of TpTc-POP and TbTc-POP after five successive photocatalysis demonstrated a few decrease in gas uptake and surface area (Fig. S8 in ESI†). However, their pore size distributions are almost consistent before and after photocatalysis. These results verified their moderate to good photochemical stabilities.

To gain insights into the reaction mechanism and the key active species involved in the photochemical conversion, several trapping experiments using different scavengers were performed as shown in Table 1. The control experiments revealed that photocatalyst TpTc, light and oxygen are all indispensable in this photo-induced reaction; otherwise, only trace conversion can be observed (Table 1, entries 2–4). Upon adding KI as the hole scavenger, a low yield of 11% was obtained (Table 1, entry 5). NaN_3 as a singlet oxygen scavenger was added into the reaction mixture, and the transformation was suppressed to some extent by NaN_3 with a yield of 47% (Table 1, entry 6). After adding *p*-benzoquinone, a typical superoxide radical anion $O_2^{\bullet-}$ scavenger, the reaction yield was greatly reduced from 95% to 20% (Table 1, entry 7). Thus, these quenching experiments imply that the hole and $O_2^{\bullet-}$ are determined as the major reactive species for this photocatalytic transformation. And the singlet oxygen can also promote the proceeding of this reaction as well. Then, electron paramagnetic resonance (EPR) measurements were performed to trap the involved reactive species of $O_2^{\bullet-}$ and $^1O_2$ by using 5,5-dimethyl-1-pyrroline-*N*-oxide (DMPO) and 2,2,6,6-tetramethylpiperidine (TEMP).[17] As expected, both $O_2^{\bullet-}$ and $^1O_2$ characteristic signals of adducts with DMPO and TEMP were observed in EPR spectra upon the irradiation of TpTc-POP in CH_3CN solution, respectively (Fig. S9 in ESI†). In addition, *N*,*N*,*N*′,*N*′-tetramethyl-phenylenediamine (TMPD) was used to detect the generation of $O_2^{\bullet-}$ from the photochemical reaction mixture.[18] As shown in Fig. 5a, a deep blue-colored solution with two strong absorption bands at 564 and 613 nm indicated the formation of the cationic radical $TMPD^{\bullet+}$ and the superoxide radical anion $O_2^{\bullet-}$ after light irradiation of TMPD solution in the presence of TpTc-POP.

Therefore, based on these above experimental results and literature reports,[18] we proposed a plausible mechanism for the photocatalytic oxidative coupling of benzylamine by POPs, as illustrated in Fig. 5b. Under the light irradiation, the polymer photocatalyst is excited to produce excitons of bound electron–

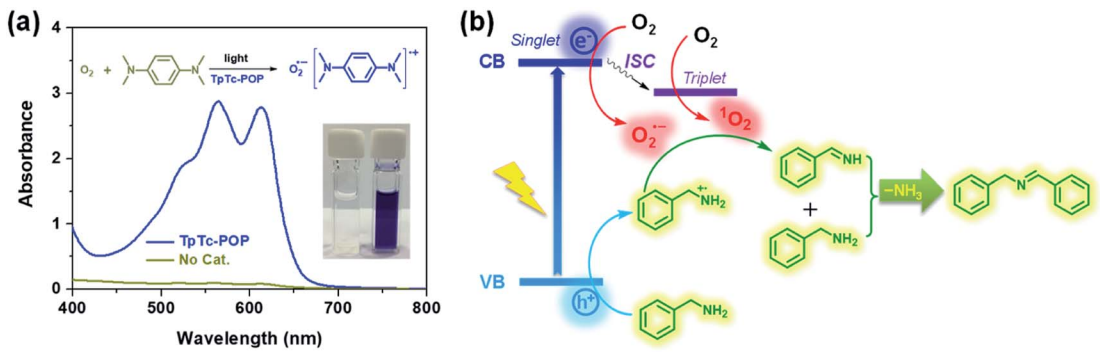

Fig. 5 (a) UV-vis spectra and photograph of the cationic radical of TMPD produced by TpTc-POP in the presence of light and oxygen. (b) The corresponding proposed mechanism for the oxidative coupling of benzylamine.

hole pairs. The photogenerated electrons can activate oxygen *via* a single electron transfer (SET) process or energy transfer, resulting in a superoxide radical $O_2^{\bullet-}$ and singlet oxygen $^1O_2$. Meanwhile, the holes are transferred to amine, producing amine radical cations. A subsequent reaction between the amine radical cation with $O_2^{\bullet-}$ and $^1O_2$ gives the intermediate imine, which can be further reacted with another amine molecule to form the desired product after removal of ammonia.

Next, the substrate scopes of oxidative coupling reactions photocatalyzed by TpTc-POP and TbTc-POP were expanded to various benzylamines with different functional groups (Tables 2 and S1 in ESI†). Various benzylamines bearing electron-donating or -withdrawing groups can be readily converted into their corresponding imine products in high yields by these two POPs photocatalysis with different reaction time. However, the electronic properties of the substituents have some effects

Table 2 Photocatalytic oxidative coupling of various amines by TpTc-POP[a]

Entry	Substrate	Product	Time (h)	Yield[b] (%)
1	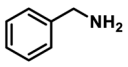	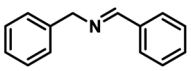	6	95
2	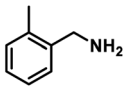	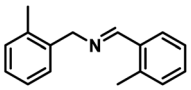	6	89
3	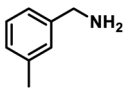	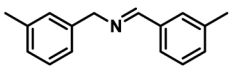	6	90
4	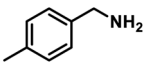	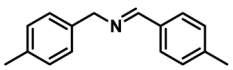	6	99
5	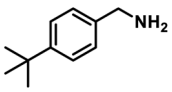	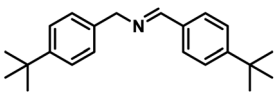	6.5	91
6	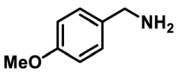	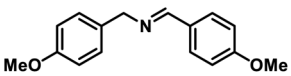	6	99
7	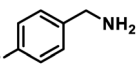	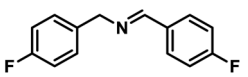	6	99
8	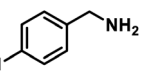	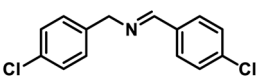	6	99
9	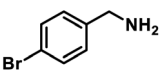	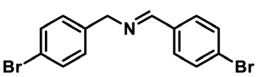	6	95
10	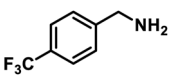	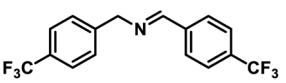	8	99
11	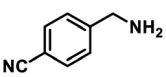	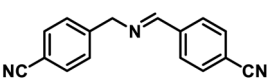	12	93
12	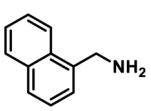	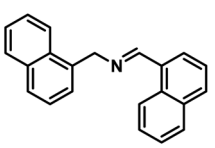	8	98
13	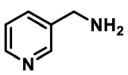	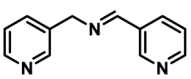	8	97
14	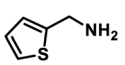	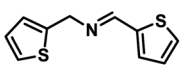	8	93

[a] Reaction conditions: benzylamines (0.5 mmol), TpTc-POP (5 mg), CH_3CN (1 mL), irradiation with white LEDs (3 W, ~100 mW cm^{-2}). [b] Determined by ^1H NMR analysis.

on the efficiency of the photocatalyzed reactions. The benzylamines with strong electron-withdrawing groups (such as $-CF_3$ and –CN, entries 10 and 11) slowed down the reaction rate and prolonged the reaction time in comparison to those with electron donating groups. Moreover, polycyclic aromatic and heterocyclic amines, such as 1-naphthalenemethylamine, 3-picolylamine and 2-thenylamine, can also be transformed into the corresponding imine with high yields (entries 12–14).

Conclusions

In summary, we have constructed two vinylene-bridged D–A structural POPs by using the electron-rich TPA and electron-deficient TCM as key building blocks and further explored their applications in photocatalytic aerobic oxidative coupling of amines to imines. The fully sp^2-carbon-connected polymer skeletons allowed for their intensive light-harvesting capabilities and tunable band structures. More importantly, due to the strong electron-donating ability of TPA units in polymers, the two POPs exhibited more impressive semiconducting properties and enhanced photocatalytic activity in comparison to the benzene-centered analogous POP. This work revealed that it is highly promising for the rational design of various D–A structural POPs with the enhanced photocatalytic performance by tuning donor and acceptor moieties at a molecular level.

Conflicts of interest

There are no conflicts to declare.

Acknowledgements

This work was financially supported from Natural Science Foundation of Jiangsu Province (BK20181001), National Natural Science Foundation of China (22001100).

References

1 (*a*) Q. Liu and L.-Z. Wu, *Natl. Sci. Rev.*, 2017, **4**, 359–380; (*b*) T. P. Yoon, M. A. Ischay and J. Du, *Nat. Chem.*, 2010, **2**, 527–532; (*c*) F. Glaser, C. Kerzig and O. S. Wenger, *Angew. Chem., Int. Ed.*, 2020, **59**, 10266–10284; (*d*) F. Strieth-Kalthoff, M. J. James, M. Teders, L. Pitzer and F. Glorius, *Chem. Soc. Rev.*, 2018, **47**, 7190–7202; (*e*) A. A. Festa, L. G. Voskressensky and E. V. Van der Eycken, *Chem. Soc. Rev.*, 2019, **48**, 4401–4423; (*f*) X.-B. Li, Z.-K. Xin, S.-G. Xia, X.-Y. Gao, C.-H. Tung and L.-Z. Wu, *Chem. Soc. Rev.*, 2020, **49**, 9028–9056; (*g*) X.-Y. Yu, J.-R. Chen and W.-J. Xiao, *Chem. Rev.*, 2021, **121**, 506–561.

2 (*a*) W. M. Cheng and R. Shang, *ACS Catal.*, 2020, **10**, 9170–9196; (*b*) F. Glaser and O. S. Wenger, *Coord. Chem. Rev.*, 2020, 405; (*c*) X.-L. Yang, J.-D. Guo, H. Xiao, K. Feng, B. Chen, C.-H. Tung and L.-Z. Wu, *Angew. Chem., Int. Ed.*, 2020, **59**, 5365–5370; (*d*) C. K. Prier, D. A. Rankic and D. W. C. MacMillan, *Chem. Rev.*, 2013, **113**, 5322–5363.

3 (*a*) N. A. Romero and D. A. Nicewicz, *Chem. Rev.*, 2016, **116**, 10075–10166; (*b*) E. Speckmeier, T. G. Fischer and K. Zeitler, *J. Am. Chem. Soc.*, 2018, **140**, 15353–15365; (*c*) C. Zhou, T. Lei, X.-Z. Wei, C. Ye, Z. Liu, B. Chen, C.-H. Tung and L.-Z. Wu, *J. Am. Chem. Soc.*, 2020, **142**, 16805–16813; (*d*) A. Srivastava, P. K. Singh, A. Ali, P. P. Singh and V. Srivastava, *RSC Adv.*, 2020, **10**, 39495–39508; (*e*) T. Ju, Y.-Q. Zhou, K.-G. Cao, Q. Fu, J.-H. Ye, G.-Q. Sun, X.-F. Liu, L. Chen, L.-L. Liao and D.-G. Yu, *Nat. Catal.*, 2021, **4**, 304–311.

4 (*a*) X. Lang, X. Chen and J. Zhao, *Chem. Soc. Rev.*, 2014, **43**, 473–486; (*b*) J. Chen, J. Cen, X. Xu and X. Li, *Catal. Sci. Technol.*, 2016, **6**, 349–362; (*c*) C. Wang, Z. Xie, K. E. deKrafft and W. Lin, *J. Am. Chem. Soc.*, 2011, **133**, 13445–13454; (*d*) Y.-Y. Zhu, G. Lan, Y. Fan, S. S. Veroneau, Y. Song, D. Micheroni and W. Lin, *Angew. Chem., Int. Ed.*, 2018, **57**, 14090–14094; (*e*) X. Lang, J. Zhao and X. Chen, *Angew. Chem., Int. Ed.*, 2016, **55**, 4697–4700; (*f*) H.-P. Liang, Q. Chen and B.-H. Han, *ACS Catal.*, 2018, **8**, 5313–5322; (*g*) L. E. Oi, M.-Y. Choo, H. V. Lee, H. C. Ong, S. B. A. Hamid and J. C. Juan, *RSC Adv.*, 2016, **6**, 108741–108754; (*h*) X. Yang, T. Huang, S. Gao and R. Cao, *J. Catal.*, 2019, **378**, 248–255.

5 (*a*) A. G. Slater and A. I. Cooper, *Science*, 2015, **348**, aaa8075; (*b*) S. Das, P. Heasman, T. Ben and S. L. Qiu, *Chem. Rev.*, 2017, **117**, 1515–1563; (*c*) Y. Yuan and G. S. Zhu, *ACS Cent. Sci.*, 2019, **5**, 409–418; (*d*) K. Geng, T. He, R. Liu, S. Dalapati, K. T. Tan, Z. Li, S. Tao, Y. Gong, Q. Jiang and D. Jiang, *Chem. Rev.*, 2020, **120**, 8814–8933; (*e*) D. Wu, F. Xu, B. Sun, R. Fu, H. He and K. Matyjaszewski, *Chem. Rev.*, 2012, **112**, 3959–4015.

6 (*a*) L. Zou, Y. Sun, S. Che, X. Yang, X. Wang, M. Bosch, Q. Wang, H. Li, M. Smith, S. Yuan, Z. Perry and H.-C. Zhou, *Adv. Mater.*, 2017, 29; (*b*) W. Ji, T.-X. Wang, X. Ding, S. Lei and B.-H. Han, *Coord. Chem. Rev.*, 2021, 439; (*c*) Q. Sun, B. Aguila, Y. Song and S. Ma, *Acc. Chem. Res.*, 2020, **53**, 812–821; (*d*) Q. Sun, Z. F. Dai, X. J. Meng and F. S. Xiao, *Chem. Soc. Rev.*, 2015, **44**, 6018–6034; (*e*) P. Zhang, S. Wang, S. Ma, F.-S. Xiao and Q. Sun, *Chem. Commun.*, 2020, **56**, 10631–10641; (*f*) D. Chen, C. Liu, J. Tang, L. Luo and G. Yu, *Polym. Chem.*, 2019, **10**, 1168–1181.

7 (*a*) Y. H. Xu, S. B. Jin, H. Xu, A. Nagai and D. L. Jiang, *Chem. Soc. Rev.*, 2013, **42**, 8012–8031; (*b*) T. Zhang, G. Xing, W. Chen and L. Chen, *Mater. Chem. Front.*, 2020, **4**, 332–353; (*c*) D. Taylor, S. J. Dalgarno, Z. Xu and F. Vilela, *Chem. Soc. Rev.*, 2020, **49**, 3981–4042; (*d*) R. Li, J. Byun, W. Huang, C. Ayed, L. Wang and K. A. I. Zhang, *ACS Catal.*, 2018, **8**, 4735–4750; (*e*) J. Byun and K. A. I. Zhang, *Mater. Horiz.*, 2020, **7**, 15–31; (*f*) T.-X. Wang, H.-P. Liang, D. A. Anito, X. Ding and B.-H. Han, *J. Mater. Chem. A*, 2020, **8**, 7003–7034; (*g*) C. Zhao, Z. Chen, R. Shi, X. Yang and T. Zhang, *Adv. Mater.*, 2020, **32**, 1907296; (*h*) C. Xu, W. Zhang, J. Tang, C. Pan and G. Yu, *Front. Chem.*, 2018, **6**, 592; (*i*) J. Xiao, X. Liu, L. Pan, C. Shi, X. Zhang and J.-J. Zou, *ACS Catal.*, 2020, **10**, 12256–12283.

8 (*a*) H. Liu, X. Yan, W. Chen, Z. Xie, S. Li, W. Chen, T. Zhang, G. Xing and L. Chen, *Sci. China: Chem.*, 2021, **64**, 827–833; (*b*) W. Li, X. Huang, T. Zeng, Y. A. Liu, W. Hu, H. Yang, Y.-B. Zhang and K. Wen, *Angew. Chem., Int. Ed.*, 2021, **60**,

1869–1874; (*c*) Y. Zhi, S. Ma, H. Xia, Y. Zhang, Z. Shi, Y. Mu and X. Liu, *Appl. Catal., B*, 2019, **244**, 36–44; (*d*) J. Luo, J. Lu and J. Zhang, *J. Mater. Chem. A*, 2018, **6**, 15154–15161.

9 (*a*) S. Xu, M. Richter and X. Feng, *Acc. Mater. Res.*, 2021, **2**, 252–265; (*b*) X. Li, *Mater. Chem. Front.*, 2021, **5**, 2931–2949; (*c*) T. He, K. Geng and D. Jiang, *Trends Chem.*, 2021, **3**, 431–444.

10 (*a*) X. Zhuang, W. Zhao, F. Zhang, Y. Cao, F. Liu, S. Bi and X. Feng, *Polym. Chem.*, 2016, **7**, 4176–4181; (*b*) E. Jin, M. Asada, Q. Xu, S. Dalapati, M. A. Addicoat, M. A. Brady, H. Xu, T. Nakamura, T. Heine, Q. Chen and D. Jiang, *Science*, 2017, **357**, 673–676.

11 (*a*) R. Chen, J.-L. Shi, Y. Ma, G. Lin, X. Lang and C. Wang, *Angew. Chem., Int. Ed.*, 2019, **58**, 6430–6434; (*b*) Y. Zhao, H. Liu, C. Wu, Z. Zhang, Q. Pan, F. Hu, R. Wang, P. Li, X. Huang and Z. Li, *Angew. Chem., Int. Ed.*, 2019, **58**, 5376–5381; (*c*) J.-L. Shi, R. Chen, H. Hao, C. Wang and X. Lang, *Angew. Chem., Int. Ed.*, 2020, **59**, 9088–9093; (*d*) E. Jin, Z. Lan, Q. Jiang, K. Geng, G. Li, X. Wang and D. Jiang, *Chem*, 2019, **5**, 1632–1647; (*e*) S. Wei, F. Zhang, W. Zhang, P. Qiang, K. Yu, X. Fu, D. Wu, S. Bi and F. Zhang, *J. Am. Chem. Soc.*, 2019, **141**, 14272–14279.

12 (*a*) S. Bi, Z.-A. Lan, S. Paasch, W. Zhang, Y. He, C. Zhang, F. Liu, D. Wu, X. Zhuang, E. Brunner, X. Wang and F. Zhang, *Adv. Funct. Mater.*, 2017, **27**, 1703146; (*b*) S. Bi, P. Thiruvengadam, S. Wei, W. Zhang, F. Zhang, L. Gao, J. Xu, D. Wu, J.-S. Chen and F. Zhang, *J. Am. Chem. Soc.*, 2020, **142**, 11893–11900; (*c*) J. Xu, C. Yang, S. Bi, W. Wang, Y. He, D. Wu, Q. Liang, X. Wang and F. Zhang, *Angew. Chem., Int. Ed.*, 2020, **59**, 23845–23853.

13 S. Li, L. Li, Y. Li, L. Dai, C. Liu, Y. Liu, J. Li, J. Lv, P. Li and B. Wang, *ACS Catal.*, 2020, **10**, 8717–8726.

14 (*a*) P. Agarwala and D. Kabra, *J. Mater. Chem. A*, 2017, **5**, 1348–1373; (*b*) Y. Lin and X. Zhan, *Acc. Chem. Res.*, 2016, **49**, 175–183; (*c*) A. Mahmood, *Sol. Energy*, 2016, **123**, 127–144; (*d*) M. Liang and J. Chen, *Chem. Soc. Rev.*, 2013, **42**, 3453–3488.

15 K. S. W. Sing, D. H. Everett, R. A. W. Haul, L. Moscou, R. A. R. Pierotti, J. Rouquérol and T. Siemieniewska, *Pure Appl. Chem.*, 1985, **57**, 603–619.

16 (*a*) Y. Xu and M. A. A. Schoonen, *Am. Mineral.*, 2000, **85**, 543–556; (*b*) S. Ghosh, N. A. Kouamé, L. Ramos, S. Remita, A. Dazzi, A. Deniset-Besseau, P. Beaunier, F. Goubard, P.-H. Aubert and H. Remita, *Nat. Mater.*, 2015, **14**, 505–511.

17 (*a*) S. Bandyopadhyay, S. Kundu, A. Giri and A. Patra, *Chem. Commun.*, 2018, **54**, 9123–9126; (*b*) S. Kundu, B. Behera, A. Giri, N. Saha and A. Patra, *Chem. Commun.*, 2021, **57**, 6875–6878.

18 (*a*) Z. J. Wang, S. Ghasimi, K. Landfester and K. A. I. Zhang, *Adv. Mater.*, 2015, **27**, 6265–6270; (*b*) Y. Zhi, K. Li, H. Xia, M. Xue, Y. Mu and X. Liu, *J. Mater. Chem. A*, 2017, **5**, 8697–8704; (*c*) Z. Li, S. Han, C. Li, P. Shao, H. Xia, H. Li, X. Chen, X. Feng and X. Liu, *J. Mater. Chem. A*, 2020, **8**, 8706–8715.